Energy Storage Materials 48 (2022) 447–457

Contents lists available at ScienceDirect

Energy Storage Materials

journal homepage: www.elsevier.com/locate/ensm

Highly reversible Mg metal anodes enabled by interfacial liquid metal engineering for high-energy Mg-S batteries

Chuanliang Wei[a], Liwen Tan[a], Yuchan Zhang[a], Baojuan Xi[b], Shenglin Xiong[b], Jinkui Feng[a,*], Yitai Qian[c]

[a] Key Laboratory for Liquid-Solid Structural Evolution and Processing of Materials (Ministry of Education), Research Center for Carbon Nanomaterials, School of Materials Science and Engineering, Shandong University, Jinan 250061, PR China
[b] School of Chemistry and Chemical Engineering, Shandong University, Jinan 250100, PR China
[c] Hefei National Laboratory for Physical Science at Microscale, Department of Chemistry, University of Science and Technology of China, Hefei 230026, PR China

ARTICLE INFO

Keywords:
Mg metal anode
Mg dendrites
Liquid metal
Alloy layer
Mg-S battery

ABSTRACT

Metallic Mg is a promising anode material for rechargeable magnesium-ion batteries (MIBs) due to its low electrochemical potential and high theoretical capacity. However, low Mg^{2+} conductivity on the interface of Mg electrode caused by liquid electrolyte passivation hinders its development. In addition, whether Mg dendrites can be formed in Mg metal anodes is controversial. Herein, we find that Mg dendrites can be formed in Mg metal anodes. The diameter of most Mg dendrites is below 100 nm, which is much smaller than Li and Na dendrites. The nanoscale Mg dendrites can easily pierce through the separators with large pore size and cause the internal short circuit of batteries. A simple strategy is proposed to address the issues of Mg metal anodes by painting a liquid metal Ga layer on Mg foil. Metallic Ga can spontaneously alloy with metallic Mg to form a stable, Mg^{2+}-conductive, corrosive-resistant, and magnesiophilic Ga_5Mg_2 alloy layer. Under the regulation of the Ga_5Mg_2 alloy layer, a highly reversible, stable, and dendrite-free Mg metal anode is obtained. Enhanced electrochemical performance is achieved both in symmetric cells and Mg-S full cells. This study paves the way for high-energy Mg-metal batteries.

1. Introduction

Lithium-ion batteries (LIBs) are considered one of the most successful energy storage devices. To date, LIBs have been widely applied in many fields such as electric vehicles, smart grids, electronic products, and energy storage stations [1–3]. However, the uneven distribution and scarcity of lithium sources in the earth crust can not only increase the cost of LIBs but also hinder their worldwide application [4,5]. To address this issue, many new battery systems have been put forward as candidates in the past several years, including sodium-ion batteries, potassium-ion batteries, calcium-ion batteries, magnesium-ion batteries (MIBs), aluminum-ion batteries, iron-ion batteries, and zinc-ion batteries [6–11].

MIBs are an attractive battery system due to the large abundance and environmental friendliness of magnesium element [12–15]. Metallic Mg is believed as a promising anode material for MIBs because of its high theoretical capacity (3833 mAh cm^{-3} or 2206 mAh g^{-1}) and low electrochemical potential (−2.37 V vs. SHE) [16–19]. Beside, metallic Mg is less reactive than metallic Li and Na, enabling it safer [20]. In addition, Mg metal anodes can pair with Mg-free cathodes such S, O_2, and CO_2 to construct high-energy Mg-metal batteries [21–23]. However, many issues restrict the practical application of Mg metal anodes. For example, Mg metal anodes can be easily corroded by liquid electrolytes due to its low electrochemical potential [24,25]. In addition, the formed passivation film on Mg metal anodes in most conventional electrolytes has poor Mg^{2+} conductivity, resulting in irreversible Mg plating/stripping process and large overpotential of batteries [26]. Furthermore, the Mg dendrite issue has been debatable until now [27–35].

Recently, various strategies have been put forward to address the interface issue of Mg metal anodes, such as adding electrolyte additives [36–40], fabricating novel electrolytes [41,42], designing artificial interface [43–55], constructing three-dimensional magnesiophilic scaffolds [56–58], theoretical research [59], exploring novel characterization methods [60], using Mg-based alloy anodes instead of pure Mg metal anodes [61,62], and replacing corrosive liquid electrolytes with solid-state electrolytes [63]. Although obvious progress has been achieved, the modification strategies for Mg metal anodes are still limited compared with those for Li metal anodes because most strategies are based on modifying electrolytes. So it is necessary and meaningful to develop novel methods to improve the stability of Mg metal anodes.

* Corresponding author.
E-mail address: jinkui@sdu.edu.cn (J. Feng).

https://doi.org/10.1016/j.ensm.2022.03.046
Received 10 January 2022; Received in revised form 25 February 2022; Accepted 28 March 2022
Available online 1 April 2022

Ga-based liquid metals such as metallic Ga, GaIn alloy, GaInSn alloy, and GaInSnZn alloy have been largely studied due to their large surface tension, superior electronic/thermal conductivity, self-healing ability, good fluidity, low melting point, and so on [64]. Recently, Ga-based liquid metals have exhibited large potential in addressing the issues of metal anodes [65,66]. However, it is still unclear whether Ga-based liquid metals can improve the stability of Mg metal anodes.

Herein, we proposed a novel strategy to boost the stability of Mg metal anodes by simply coating a thin liquid metal Ga layer on Mg foil. After coating, the liquid metal Ga layer could immediately alloy with the underneath metallic Mg to form a Ga_5Mg_2 alloy layer at room temperature. The strategy proposed here exhibits several merits. First, the liquid metal coating method was simple. Second, the Ga_5Mg_2 alloy layer could be tightly coated on the surface of Mg foil, without shedding even under bending, folding, heating, and plating/stripping. Third, the Ga_5Mg_2 alloy layer had lower chemical reactivity than pure Mg foil, and it could act as a protective layer for the underneath Mg foil to relieve the interfacial corrosion and promote the reversible Mg plating/stripping. Fourth, Ga_5Mg_2 alloy was a mixed ion/electron conductor, which could enable fast electrochemical kinetics on the interface. In Ga_5Mg_2 compound, theoretical calculation indicated that the Mg cations transferred electrons around the Ga atoms, and covalent bonds were formed between Mg–Ga atoms [67]. The transfer of Mg atoms to the Mg–Ga bond was about 2.0 e^- per atom. In addition, Ga_5Mg_2 had a large density of states at the Fermi level, which indicated a superior metallic property. So Ga_5Mg_2 alloy owned fast electron transport kinetics and electron conductivity. Theoretical calculation also revealed Ga_5Mg_2 alloy had a low diffusion energy barrier of 1.91 and 2.55 eV for intra-layer and cross-layer diffusion, indicating a fast Mg^{2+} diffusion ability. Fifth, the phase composition of Ga_5Mg_2 alloy layer could keep stable during the Mg plating/stripping process. Sixth, Ga_5Mg_2 alloy exhibited a certain magnesiophilicity due to the existence of magnesiophilic Ga sites, which could reduce the nucleation barrier and homogenize Mg^{2+} flux during the Mg plating/stripping process, resulting in uniform and dendrite-free Mg deposition.

2. Experimental section

2.1. Chemicals and materials

Mg foil (50 μm in thickness) was purchased from Xinwang Scientific Research Metal Materials Co., Ltd., China. Liquid metal Ga was purchased from Yunnan Zhongxuan Liquid Metal Technology Co., Ltd., China. Stainless steel foil (SSF, Q235, 30 μm in thickness) was bought from Xinwang Scientific Research Metal Materials Co., Ltd., China. All the experiments were proceed at room temperature.

2.2. Preparation of Ga_5Mg_2 alloy coated Mg foil (Ga_5Mg_2-Mg)

First, solid-state metallic Ga was heated to be liquid state using a hot plate. Then the Mg foil was polished by a sandpaper to remove the surface natural passivation layer. Afterwards, the polished Mg foil was cleaned by an air-laid paper to remove the surface impurities. Subsequently, liquid-state Ga was quickly and uniformly coated on the

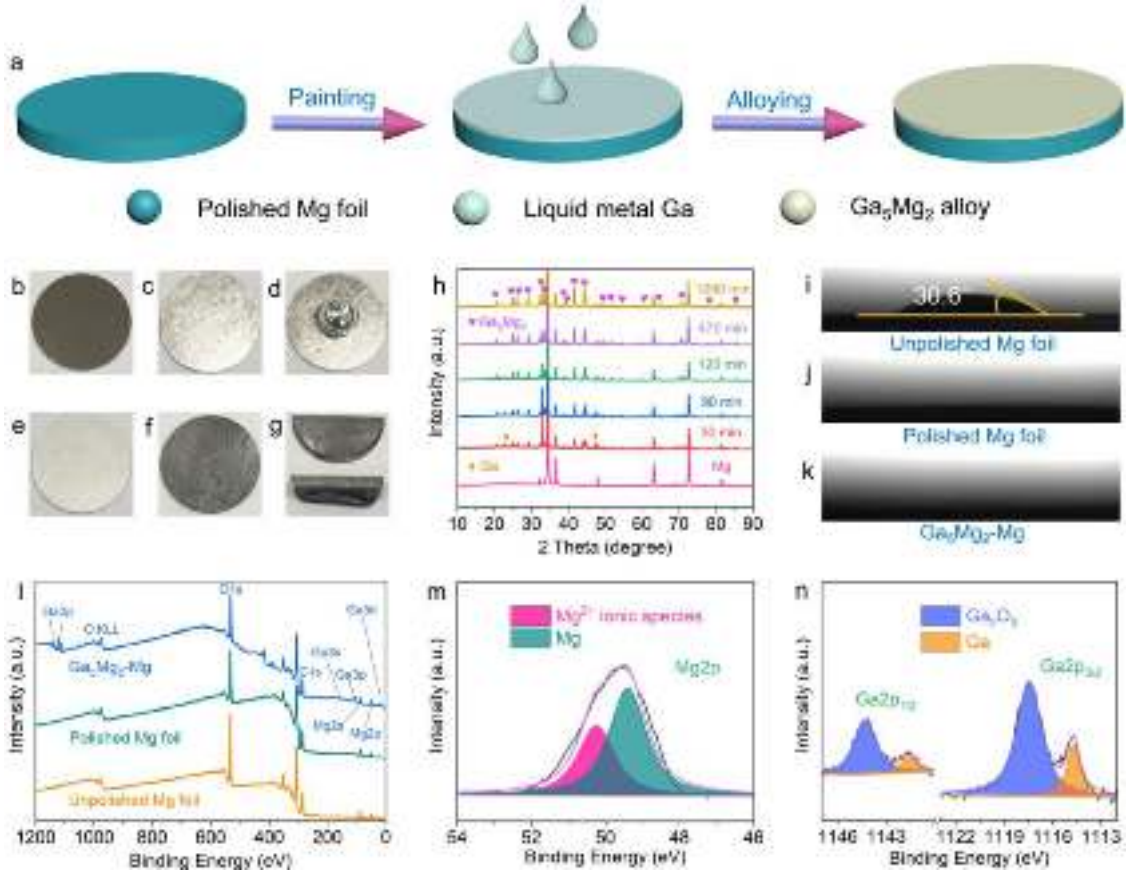

Fig. 1. (a) A schematic showing the fabrication process of Ga_5Mg_2-Mg. (b) A photograph of unpolished Mg foil with a diameter of 16 mm. (c) A photograph of polished Mg foil. (d) A photograph after dropping a drop of liquid-state Ga on polished Mg foil. (e) A photograph after painting liquid-state Ga on polished Mg foil. (f) A photograph of Ga_5Mg_2-Mg. (g) A photograph showing the bendable and foldable Ga_5Mg_2-Mg. (h) XRD patterns of polished Mg foil and liquid metal Ga coated Mg foil after different alloying time. (i–k) Contact angle of liquid electrolyte on unpolished Mg foil, polished Mg foil, and Ga_5Mg_2-Mg, respectively. (l) XPS full spectra of unpolished Mg foil, polished Mg foil, and Ga_5Mg_2-Mg. (m) High-resolution XPS spectra of Mg2p in Ga_5Mg_2-Mg. (n) High-resolution XPS spectra of Ga2p in Ga_5Mg_2-Mg.

surface of the polished Mg foil using a small brush. Then the liquid metal coated Mg foil was immediately transferred into the Ar-filled glove box (O_2<0.01 ppm, H_2O<0.01 ppm) to proceed the alloying reaction. Finally, the Ga_5Mg_2-Mg was obtained after spontaneously alloying for 24 h. The mass loading of liquid metal Ga on Mg foil was 0.5–0.8 mg cm^{-2}.

2.3. Preparation of Ketjen black/S (KB/S) composite

The KB/S composite was prepared by a melt-diffusion method. First, KB and S powders (4:6 in mass ratio) were mixed and grounded in an agate mortar for 30 min. Then the mixture was heated at 155 ˚C for 10 h in an Ar atmosphere. After cooling down, the KB/S composite was obtained.

2.4. Sample characterization

X-ray diffraction (XRD, MiniFlex 600, Cu-Kα radiation, Japan) was performed to investigate the phase compositions and changes of samples. Scanning electron microscope (SEM, JSM-7610F, Japan) was utilized to observe the morphology of samples. Energy dispersive spectrometer (X-max, England) was used to obtain the energy-dispersive spectroscopy (EDS) mapping of elements in samples. X-ray photoelectron spectroscopy (XPS, Axis Supra, Al-Kα source, Japan) was used to probe the chemical states of elements in samples. Contact angle measurement instrument (JC2000D1, China) was utilized to observe the contact angle between liquid electrolyte and samples.

2.5. Electrochemical measurements

2032-type coin cells were used to investigate the electrochemical performance of samples. The cells were assembled in an Ar-filled glove box (O_2<0.01 ppm, H_2O<0.01 ppm). A piece of glass fiber film (Whatman) sandwiched between two pieces of polyethylene films (Celgard) was utilized as the separator. 0.5 M $Mg(TFSI)_2$ in DME with 20 wt% 1-methoxy-2-propylamine was used as the liquid electrolyte. The electrolyte was prepared according to a previous report [37]. 1-methoxy-2-propylamine was a chelant, which could reduce the side reactions on Mg

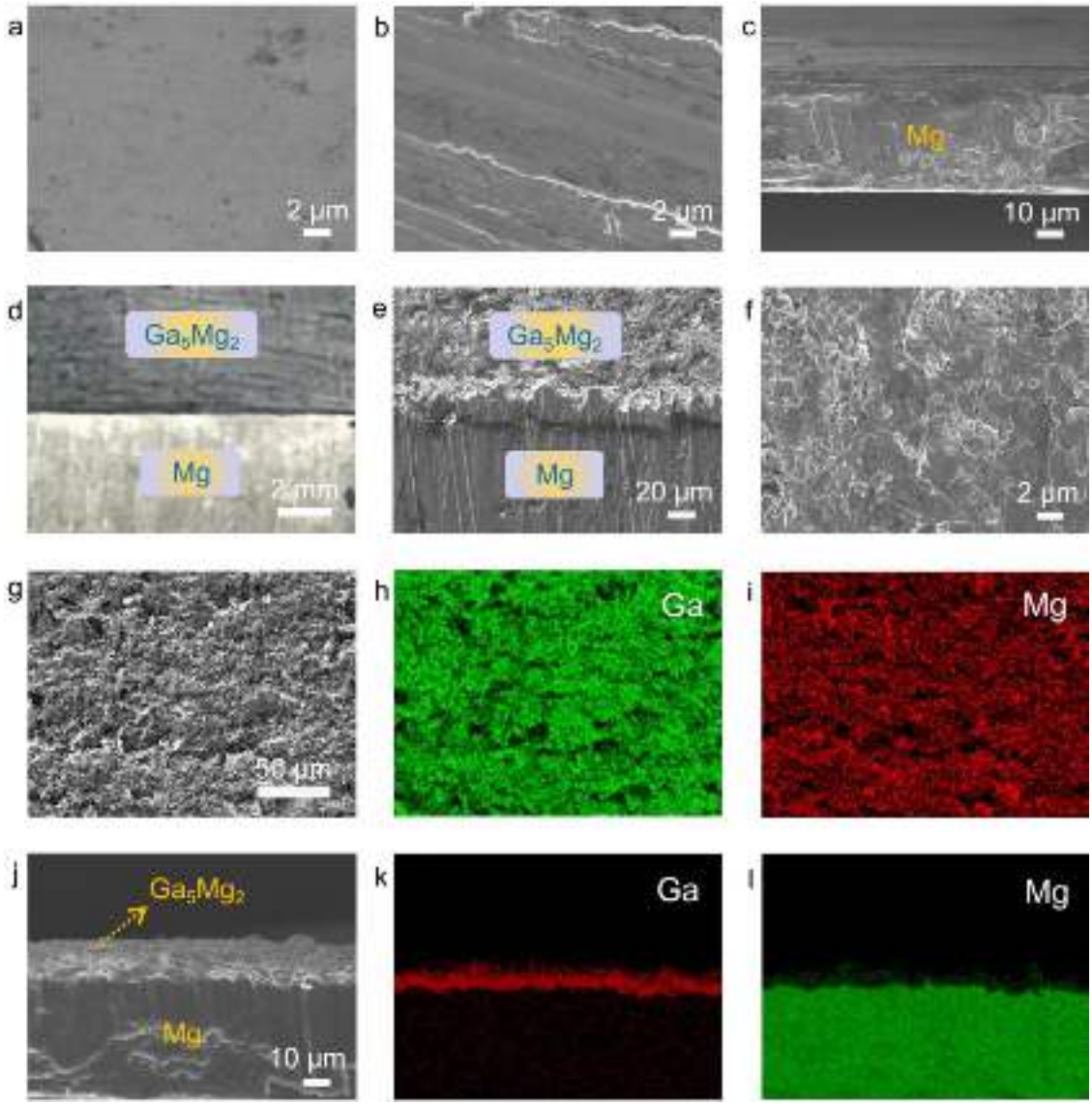

Fig. 2. (a, b) Top-view SEM images of unpolished Mg foil and polished Mg foil, respectively. (c) Cross-sectional SEM image of polished Mg foil. (d) A photograph of partial Ga_5Mg_2 coated Mg foil. (e) Top-view SEM image of partial Ga_5Mg_2 coated Mg foil. (f) Top-view SEM image of Ga_5Mg_2-Mg. (g–i) Top-view SEM image of Ga_5Mg_2-Mg and corresponding EDS mapping of Ga and Mg elements. (j–l) Cross-sectional SEM image of Ga_5Mg_2-Mg and corresponding EDS mapping of Ga and Mg elements.

metal anode and accelerate the interfacial charge transfer kinetics via solvation sheath reorganization [37]. Bare 0.5 M $Mg(TFSI)_2$/DME electrolyte usually resulted in a large overpotential of batteries due to the serious interfacial corrosion and passivation [37]. The amount of liquid electrolyte used in each coin cell was 200 μL. To prepare the working electrodes, polished Mg foil and Ga_5Mg_2-Mg were punched to be slices (1 cm in diameter). CT-4008 Neware battery testers were used to control the charge-discharge processes of cells. A CHI660E electrochemical workstation was utilized to test the electrochemical impedance spectroscopy (EIS) and cyclic voltammetry (CV).

The cycling performance of symmetric cells was tested at different current densities and capacities using two same electrodes (Mg or Ga_5Mg_2-Mg). The electrochemical performance of Mg-S full cells was tested using KB/S as the cathode and Mg or Ga_5Mg_2-Mg as the anode. To fabricate the KB/S cathode, KB/S powders, super-P, and PVDF were mixed with a mass ratio of 7:2:1 in NMP solvent to form a uniform slurry. Then the KB/S cathode was achieved by pasting the slurry on a piece of Al foil followed by a vacuum drying process at 60 ˚C. Finally, the KB/S cathode was punched to be disks (1 cm in diameter). The mass loading of S was about 0.5 mg cm^{-2}. The charge-discharge performance of Mg-S full cells was tested at 0.1 C (1 C=1675 mA g^{-1}) in 0.1–2.5 V. The liquid electrolyte used for Li deposition was 1 M LiTFSI in DOL/DME (1:1 by volume). The liquid electrolyte used for Na deposition was 1 M $NaPF_6$ in EC/DEC (1:1 by volume) with 5% FEC.

3. Results and discussion

The Ga_5Mg_2-Mg was prepared by simply painting a liquid metal Ga layer on polished Mg foil followed by a spontaneous alloying process at room temperature (Fig. 1a). Metallic Ga has a melting point of 29.8 ˚C and it exhibits a solid state at room temperature (Fig. S1a). After a heat treatment, solid-state Ga could be changed to be liquid-state Ga (Fig. S1b), which could be easily painted on the polished Mg foil. The unpolished Mg foil showed a dusky surface due to the existence of surface natural passivation layer (Fig. 1b), which mainly contained MgO, $Mg(OH)_2$, and $MgCO_3$. The surface natural passivation layer could be removed by a sandpaper. Bright metal luster and marks of polishing were observed on the polished Mg foil (Fig. 1c). Metallic Ga showed a ball-like shape after dropping a drop of liquid-state Ga on the polished Mg foil, which should be attributed to the high-surface tension of liquid metal (Fig. 1d).

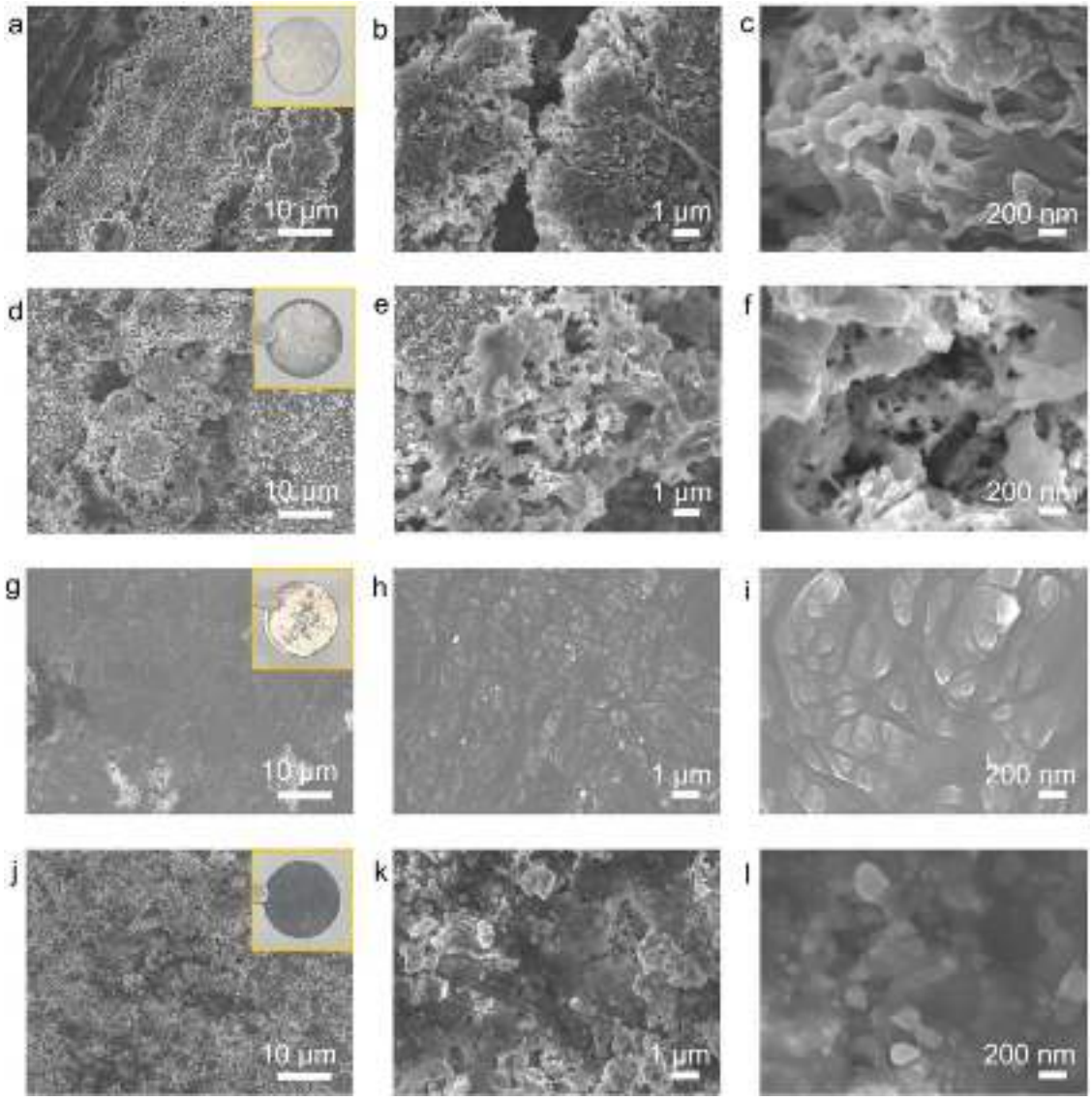

Fig. 3. (a–c) Top-view SEM images after plating 0.5 mAh cm^{-2} of Mg on Mg electrode at 0.5 mA cm^{-2}. (d–f) Top-view SEM images after stripping 0.5 mAh cm^{-2} of Mg from Mg electrode at 0.5 mA cm^{-2}. (g–i) Top-view SEM images after plating 0.5 mAh cm^{-2} of Mg on Ga_5Mg_2-Mg electrode at 0.5 mA cm^{-2}. (j–l) Top-view SEM images after stripping 0.5 mAh cm^{-2} of Mg from Ga_5Mg_2-Mg electrode at 0.5 mA cm^{-2}.

Liquid-state Ga could be easily spread on the surface of polished Mg foil by using a small brush (Fig. 1e). After placing the liquid metal coated Mg foil in a glove box for 24 h, the surface became gray, indicating the formation of the alloy layer (Fig. 1f). The alloy layer could be tightly attached on Mg foil even under bending and folding (Fig. 1g).

XRD was used to probe the phase compositions and changes of the liquid metal coated Mg foil during the alloying process (Fig. 1h). When the alloying time was 30 min, diffraction peaks of metallic Mg, metallic Ga, and Ga_5Mg_2 alloy were observed. With the increase of the alloying time (30 to 120 min), the intensity of diffraction peaks belonging to metallic Ga was gradually weakened, indicating metallic Ga was transformed into Ga_5Mg_2 alloy gradually. The diffraction peaks of metallic Ga disappeared when the alloying time was 470 min. In addition, when further increasing the alloying time to 1080 min, the kinds of diffraction peaks were similar with those at 470 min, indicating metallic Ga was fully transformed into Ga_5Mg_2 alloy.

Contact angle was tested to investigate the wettability of liquid electrolyte with substrates (Fig. 1i–k). The contact angle of liquid electrolyte on unpolished Mg foil, polished Mg foil, and Ga_5Mg_2-Mg was 30.6°, 0°, and 0°, respectively. The dense surface natural passivation layer on unpolished Mg foil could block the infiltration of liquid electrolyte, which could explain its higher contact angle. XPS full spectra showed the intensity of O element in polished Mg foil was reduced compared with that in unpolished Mg foil, indicating polishing with sandpapers could remove the surface natural passivation layer (Fig. 1l). In addition, Ga and Mg elements were detected on the surface of Ga_5Mg_2-Mg. High-resolution XPS spectra were presented to investigate the chemical state of Ga and Mg elements on Ga_5Mg_2-Mg. The binding energies of Mg2p at around 49.40 and 50.25 eV were attributed to metallic Mg and Mg^{2+} ionic species (MgO, $Mg(OH)_2$, etc.), respectively (Fig. 1m) [58]. The binding energies of Ga2p at about 1144.32 (1117.45) and 1141.60 (1114.70) eV were attributed to Ga_2O_3 and Ga, respectively (Fig. 1n) [66]. A thin oxide layer could be easily formed on the surface of metals, which could explain the existence of MgO and Ga_2O_3 on Ga_5Mg_2-Mg [68].

SEM images of the unpolished Mg foil showed that a natural passivation layer was covered on the surface (Figs. 2a, S2a). After polished with a sandpaper, the surface natural passivation layer was removed and the underneath fresh metallic Mg appeared (Figs. 2b,c, S2b, S3a). In addition, obvious polishing marks were observed. A partial Ga_5Mg_2 coated Mg foil showed an obvious boundary (Fig. 2d,e). A linear scanning indicated that the bottom was fresh Mg and the top was Ga_5Mg_2 alloy layer (Fig. S4). Top-view and cross-sectional SEM images of Ga_5Mg_2-Mg showed that the Ga_5Mg_2 alloy layer was successfully formed on the surface (Figs. 2f–l, S2c, S3b,c). The thickness of the alloy layer was about 4,5 μm. It should be noted that a too thin alloy layer could not effectively resist the corrosion by liquid electrolyte. A too thick alloy layer could affect the electrochemical behaviors of the composite anode, which had been carefully studied by previous reports [61,62]. Both cases could affect the electrochemical performance of batteries. Top-view SEM images indicated the Ga_5Mg_2 alloy layer was rough, and some particles and pores were observed on it. Cross-sectional SEM images showed that the Ga_5Mg_2 alloy layer was tightly attached on the top surface of metallic

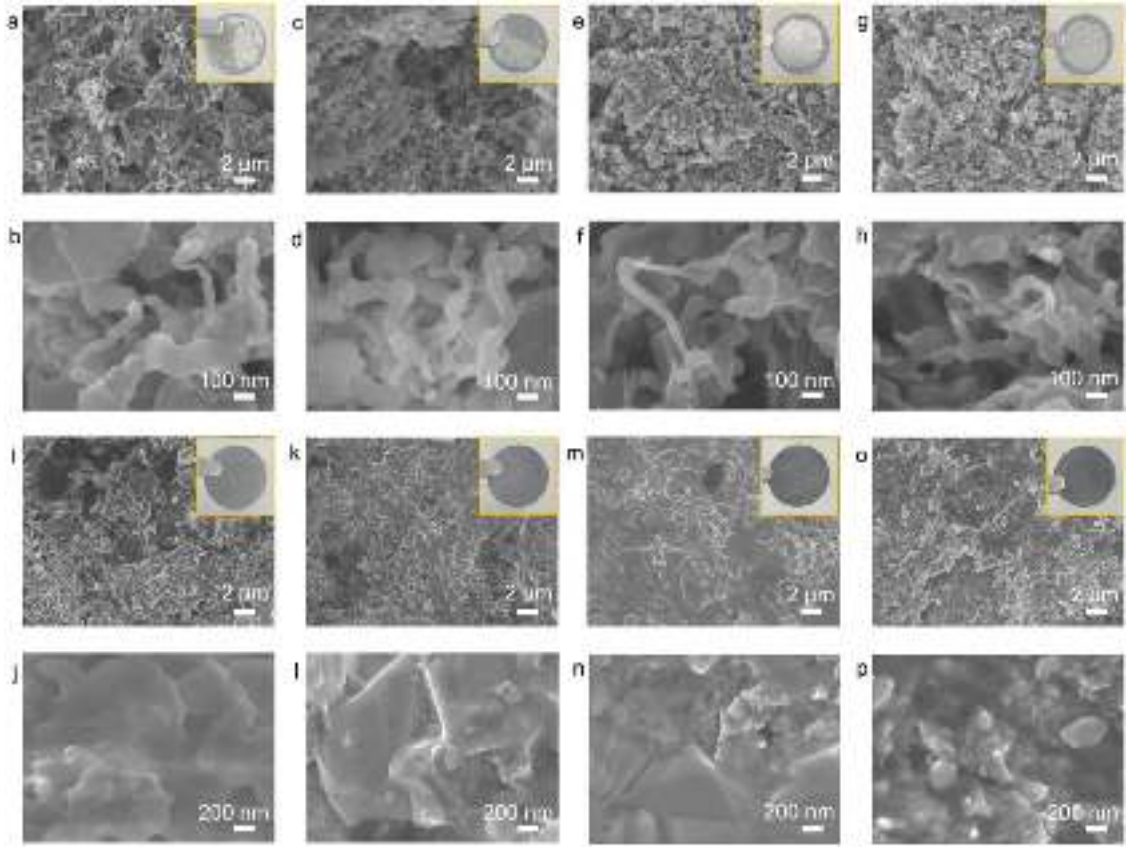

Fig. 4. (a, b) Top-view SEM images of Mg electrode after 10 plating/stripping cycles in symmetric cells (0.5 mA cm^{-2}-0.5 mAh cm^{-2}). (c, d) Top-view SEM images of Mg electrode after 10 stripping/plating cycles in symmetric cells (0.5 mA cm^{-2}-0.5 mAh cm^{-2}). (e, f) Top-view SEM images of Mg electrode after 30 plating/stripping cycles in symmetric cells (0.5 mA cm^{-2}-0.5 mAh cm^{-2}). (g, h) Top-view SEM images of Mg electrode after 30 stripping/plating cycles in symmetric cells (0.5 mA cm^{-2}-0.5 mAh cm^{-2}). (i, j) Top-view SEM images of Ga_5Mg_2-Mg electrode after 10 plating/stripping cycles in symmetric cells (0.5 mA cm^{-2}-0.5 mAh cm^{-2}). (k, l) Top-view SEM images of Ga_5Mg_2-Mg electrode after 10 stripping/plating cycles in symmetric cells (0.5 mA cm^{-2}-0.5 mAh cm^{-2}). (m, n) Top-view SEM images of Ga_5Mg_2-Mg electrode after 30 plating/stripping cycles in symmetric cells (0.5 mA cm^{-2}-0.5 mAh cm^{-2}). (o, p) Top-view SEM images of Ga_5Mg_2-Mg electrode after 30 stripping/plating cycles in symmetric cells (0.5 mA cm^{-2}-0.5 mAh cm^{-2}).

Mg. EDS elemental distribution mapping indicated Ga and Mg elements were uniformly distributed on the surface.

The surface morphology of electrodes after Mg plating or stripping was investigated. Uneven and dendritic Mg deposition was observed after plating 0.5 mAh cm^{-2} of Mg on Mg electrode at 0.5 mA cm^{-2} (Fig. 3a–c). Differently, uniform and dendrite-free Mg deposition was formed on Ga_5Mg_2-Mg (Figs. 3g–i, S5). After deposition, the surface of Ga_5Mg_2-Mg electrode turned from gray to bright metal luster (Inset in Fig. 3g). The SEM image indicated that the surface morphology of Ga_5Mg_2-Mg electrode after deposition (Fig. 3g) became smooth compared with the electrode before deposition (Fig. S2c). These results combined with the EDS mapping

Fig. S5 showed that Mg was deposited on the surface of Ga_5Mg_2-Mg electrode. Ga_5Mg_2 alloy was a mixed ion/electron conductor. However, the Ga_5Mg_2 alloy exhibited a metal-level electronic conductivity and thus Mg^{2+} could easily accept electron on the surface of Ga_5Mg_2-Mg electrode to form metallic Mg in the plating process. So Mg was deposited on the surface instead of below the Ga_5Mg_2 alloy layer. This deposition phenomenon has been reported in Li metal anodes [65]. The surface of Mg electrode was porous and dendritic after stripping 0.5 mAh cm^{-2} of Mg (Fig. 3d–f). While the surface of Ga_5Mg_2-Mg electrode after stripping was similar with the electrode before stripping, without formation of Mg dendrites (Fig. 3j–l).

The surface morphology of electrodes after different cycles in symmetric cells was observed by SEM. The surface of Mg electrodes became rough and porous after cycling, which was quite different from the electrodes before cycling (Fig. 4a–h). Obvious Mg dendrites were detected on Mg electrodes after 10 and 30 plating/stripping (or stripping/plating) cycles. In contrast, the surface of Ga_5Mg_2-Mg electrodes after cycling was similar with the electrodes before cycling (Fig. 4i–p). Enlarged SEM images showed that no Mg dendrites were observed on Ga_5Mg_2-Mg electrodes after cycling. These SEM results indicated the Ga_5Mg_2 layer could inhibit the formation of Mg dendrites.

The stability of Ga_5Mg_2-Mg was investigated. After immersed in liquid electrolyte for 72 h, the surface of Mg electrode became rough and

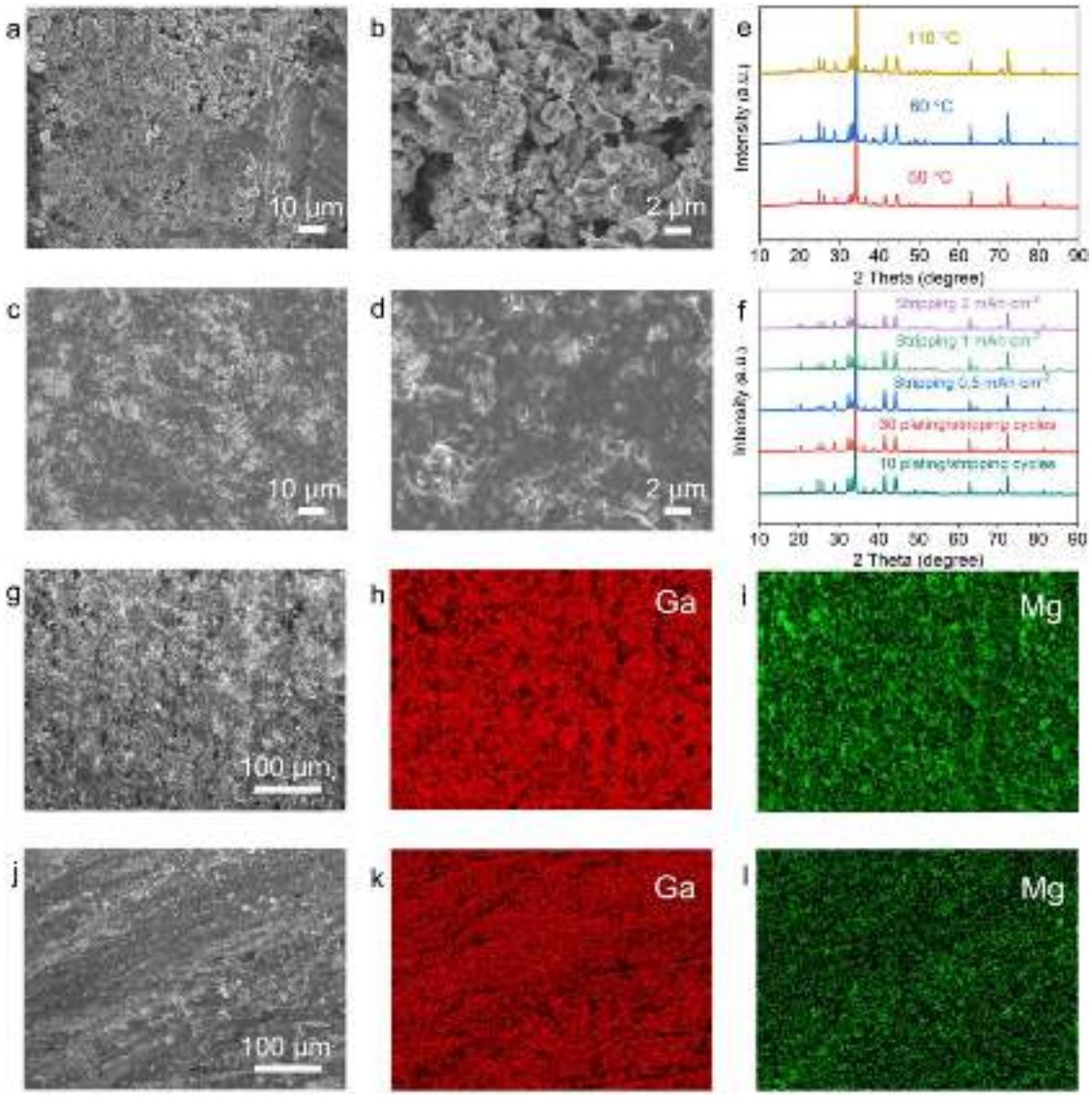

Fig. 5. (a, b) Top-view SEM images of Mg electrode after immersed in liquid electrolyte for 72 h. (c, d) Top-view SEM images of Ga_5Mg_2-Mg electrode after immersed in liquid electrolyte for 72 h. (e) XRD patterns of Ga_5Mg_2-Mg after heated in an Ar atmosphere for 1 h at different temperatures. (f) XRD patterns of Ga_5Mg_2-Mg electrode after different electrochemical processes. (g–i) Top-view SEM image of Ga_5Mg_2-Mg electrode after 10 plating/stripping cycles (0.5 mA cm^{-2}-0.5 mAh cm^{-2}) and corresponding EDS mapping of Ga and Mg elements. (j–l) Top-view SEM image of Ga_5Mg_2-Mg electrode after 10 stripping/plating cycles (0.5 mA cm^{-2}-0.5 mAh cm^{-2}) and corresponding EDS mapping of Ga and Mg elements.

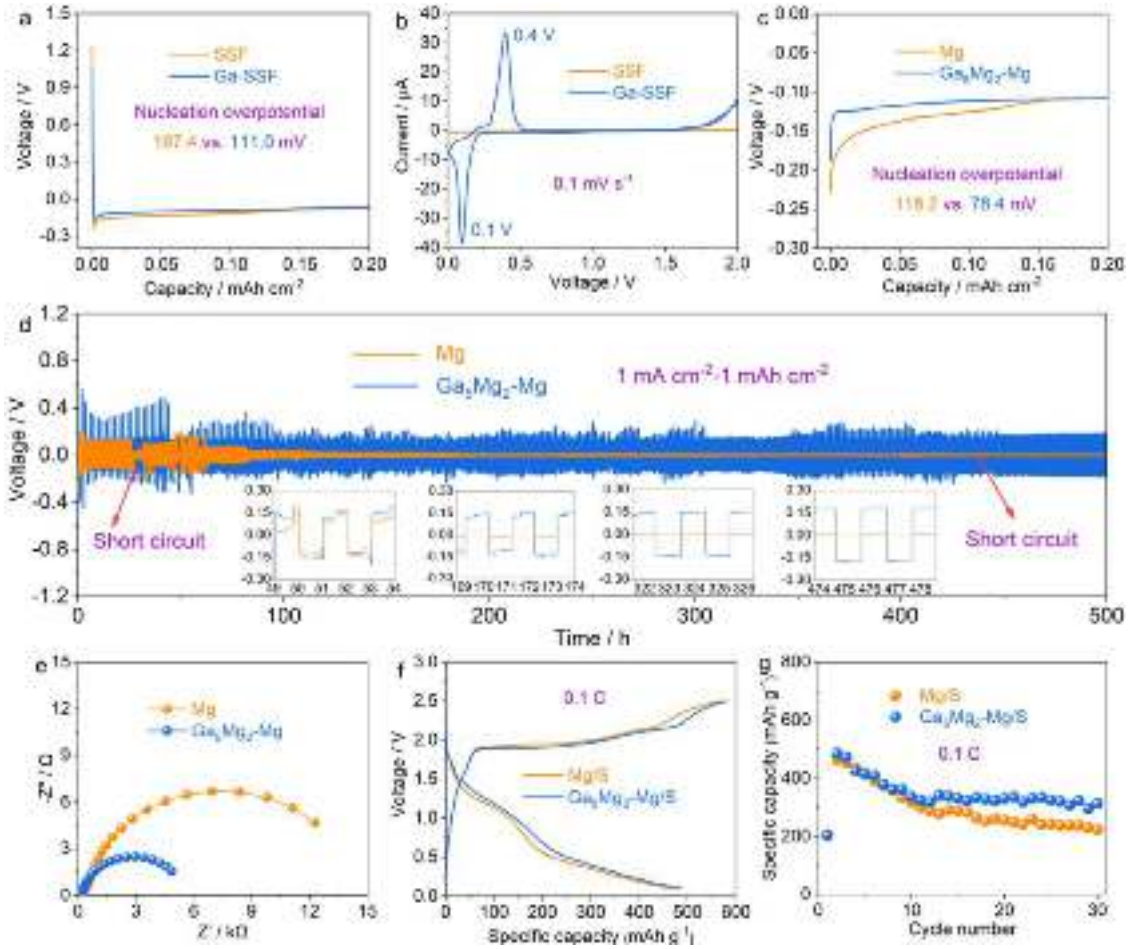

Fig. 6. (a) Voltage-capacity curves showing the nucleation overpotential of Mg on SSF and Ga-SSF at 0.05 mA cm^{-2}. (b) CV curves of SSF and Ga-SSF at 0.1 mV s^{-1} in 0.01–2 V. (c) Voltage-capacity curves showing the nucleation overpotential of Mg on Mg and Ga_5Mg_2-Mg electrodes at 0.2 mA cm^{-2}. (d) Voltage-time curves of Mg and Ga_5Mg_2-Mg symmetric cells. (e) Nyquist plots of Mg and Ga_5Mg_2-Mg symmetric cells. (f) The second charge-discharge curves of Mg/S and Ga_5Mg_2-Mg/S full cells at 0.1 C. (g) Cycling performance of Mg/S and Ga_5Mg_2-Mg/S full cells at 0.1 C.

porous, which was due to the serious corrosion by liquid electrolyte (Figs. 5a,b, S6a). The internal reason for the corrosion of Mg electrode was the low electrochemical potential of metallic Mg (−2.37 V vs. SHE), which resulted in a high chemical reactivity of Mg metal anodes. In contrast, no obvious changes were found for Ga_5Mg_2-Mg after immersion, indicating the Ga_5Mg_2 layer was corrosive-resistant (Figs. 5c,d, S6b). The exposed high-reactive Mg sites were obviously reduced on the surface of Ga_5Mg_2-Mg electrode compared with pure Mg electrode. So the corrosion was relieved for Ga_5Mg_2-Mg electrode. In fact, alloy anodes have been proved to own lower chemical reactivity than pure metal anodes [69–71]. After heated in an Ar atmosphere for 1 h at different temperatures (50, 80, and 110 °C), the phase composition and structure of Ga_5Mg_2-Mg did not suffer obvious changes (Figs. 5e, S7), which indicated the thermal stability of Ga_5Mg_2-Mg was satisfactory. The phase composition of Ga_5Mg_2-Mg could still keep stable even after stripping different amount (0.5, 1, and 2 mAh cm^{-2}) of Mg or undergoing various plating/stripping cycles (10 and 30) (Figs. 5f, S8). EDS mapping indicated that Ga and Mg elements could still exist on the surface of Ga_5Mg_2-Mg after 10 plating/stripping or stripping/plating cycles (Fig. 5g–l). These results indicated that Ga_5Mg_2-Mg owned superior stability.

To verify the magnesiophilicity of metallic Ga, the nucleation overpotential of SSF and Ga-coated SSF (Ga-SSF) was tested (Fig. 6a). The Ga-SSF was prepared by painting liquid-state Ga on SSF. The mass loading of liquid metal Ga on SSF was 0.8–1.2 mg cm^{-2}. SSF was selected to paint Ga due to its stability with Ga at room temperature [72]. The nucleation overpotential of Mg on SSF and Ga-SSF was 167.4 and 111.0 mV at 0.05 mA cm^{-2}, respectively. CV was used to further probe the magnesiophilicity of metallic Ga. No obvious redox peaks were found in the CV curves of SSF (Figs. 6b, S9). In contrast, a pair of obvious redox peaks were observed in the CV curves of Ga-SSF. These results indicated metallic Ga was magnesiophilic and could lower the nucleation overpotential of Mg in the plating process. To investigate the magnesiophilicity of Ga_5Mg_2 layer, the nucleation overpotential of Mg on Mg and Ga_5Mg_2-Mg electrodes was tested at 0.2 mA cm^{-2} (Fig. 6c). The voltage of Ga_5Mg_2-Mg electrode became flat more quickly than that of Mg electrode, indicating an easier nucleation behavior. The nucleation overpotential was 118.2 and 78.4 mV for Mg and Ga_5Mg_2-Mg electrodes, respectively. The existence of magnesiophilic Ga sites in Ga_5Mg_2 layer and its corrosive-resistant ability leaded to a lower Mg nucleation overpotential. While for bare Mg electrode, the passivated surface caused by corrosion increased the Mg nucleation barrier and thus resulted in a large nucleation overpotential. Symmetric cells were used to probe the cycling stability of electrodes (1 mA cm^{-2}-1 mAh cm^{-2}) (Fig. 6d). The voltage of Mg symmetric cell suddenly dropped to a very small value at about 27 h, indicating the occurrence of short-circuit, which was caused by the formation of Mg dendrites. From then on, the Mg symmetric cell kept short-circuited in most cycling time because the voltage-time curves presented rectangular shapes with very low overpotential [60]. In contrast, the Ga_5Mg_2-Mg symmetric cell could last

for 500 h without short circuit. The voltage fluctuation of Ga_5Mg_2-Mg symmetric cell during the cycling process should be attributed to the interfacial unstability of Mg-based electrodes in DME based electrolytes, which had been proved by previous reports [37,45]. Mg-Mg symmetric cells using two polyethylene separators were also investigated (Fig. S10). The voltage of Mg deposition curves was unstable. In addition, the Mg deposition curves exhibited a rapid voltage change in the first cycle. According to previous reports, these phenomenons could be attributed to the micro short circuit of cells [32]. The micro short circuit of cells could be caused by burrs in Mg electrodes or the easy formation of dendrites in the electrolyte used in this research. The burrs in Mg electrodes were usually formed in the punch process. To eliminate the effect of burrs in Mg electrodes, a piece of glass fiber film (Whatman) sandwiched between two pieces of polyethylene films (Celgard) was utilized as the separator in this research. This separator was thick enough to eliminate the effect of burrs in Mg electrodes. The EIS was presented to evaluate the impedance of symmetric cells (Fig. 6e). The impedance of Mg symmetric cells was much higher than that of Ga_5Mg_2-Mg symmetric cells, which was attributed to the severe corrosion of Mg electrode by liquid electrolyte. The corrosion from liquid electrolyte could passivate the surface of Mg electrode and block the transport of ions, resulting in a large impedance. While for Ga_5Mg_2-Mg electrode, the corrosive-resistant Ga_5Mg_2 alloy layer could protect the underneath Mg from corrosion.

S is a promising cathode material for MIBs [73,74]. Mg-S full cells were assembled to evaluate the practical application ability Ga_5Mg_2-Mg electrode by using KB/S composite as the cathode material (Figs. S11–S13). The discharge specific capacity of the first cycle was low for Mg/S and Ga_5Mg_2-Mg/S cell due to the necessary activation of S electrode [75]. The discharge plateau was not obvious due to the large polarization, which could be attributed to the sluggish electrochemical kinetics of polysulfide conversion [76,77]. The polarization could be reduced by improving the electrical conductivity of electrode materials or adding special catalysts [78,79]. All in all, here Mg-S cells were studied based on a proof of concept. More detail work should be proceed in the future. The discharge specific capacity of the second cycle was 485.2 mAh g^{-1} for Ga_5Mg_2-Mg/S cell (Fig. 6f). After 30 cycles at 0.1 C, the discharge specific capacity was 312.2 mAh g^{-1} (Fig. 6g). While for Mg/S cell, the discharge specific capacity decreased from 464.6 (the second cycle) to 223.2 mAh g^{-1} after 30 cycles at 0.1 C. So Ga_5Mg_2-Mg/S cell exhibited a better cycling performance than Mg/S cell. The dissolution of polysulfides in electrolytes was a serious problem for Mg-S batteries [80]. For Mg/S cell, the dissolved polysulfides during the cycling process could easily react with metallic Mg (Figs. S14,S15), which could not only endlessly consume polysulfides but also passivate the Mg electrode, finally resulting in a poor cycling performance. Differently, the Ga_5Mg_2-Mg electrode was corrosive-resistant, which could relieve the corrosion and reduce the consumption of polysulfides (Figs. S14,S15). The decomposition of electrolytes could form a passivation layer on Mg and Ga_5Mg_2-Mg electrodes. The passivation layer mainly contained elements such as C, O, and S [37]. EDS mapping of Mg and Ga_5Mg_2-Mg electrodes after cycling showed the content of C, O, and S on Mg electrode was higher

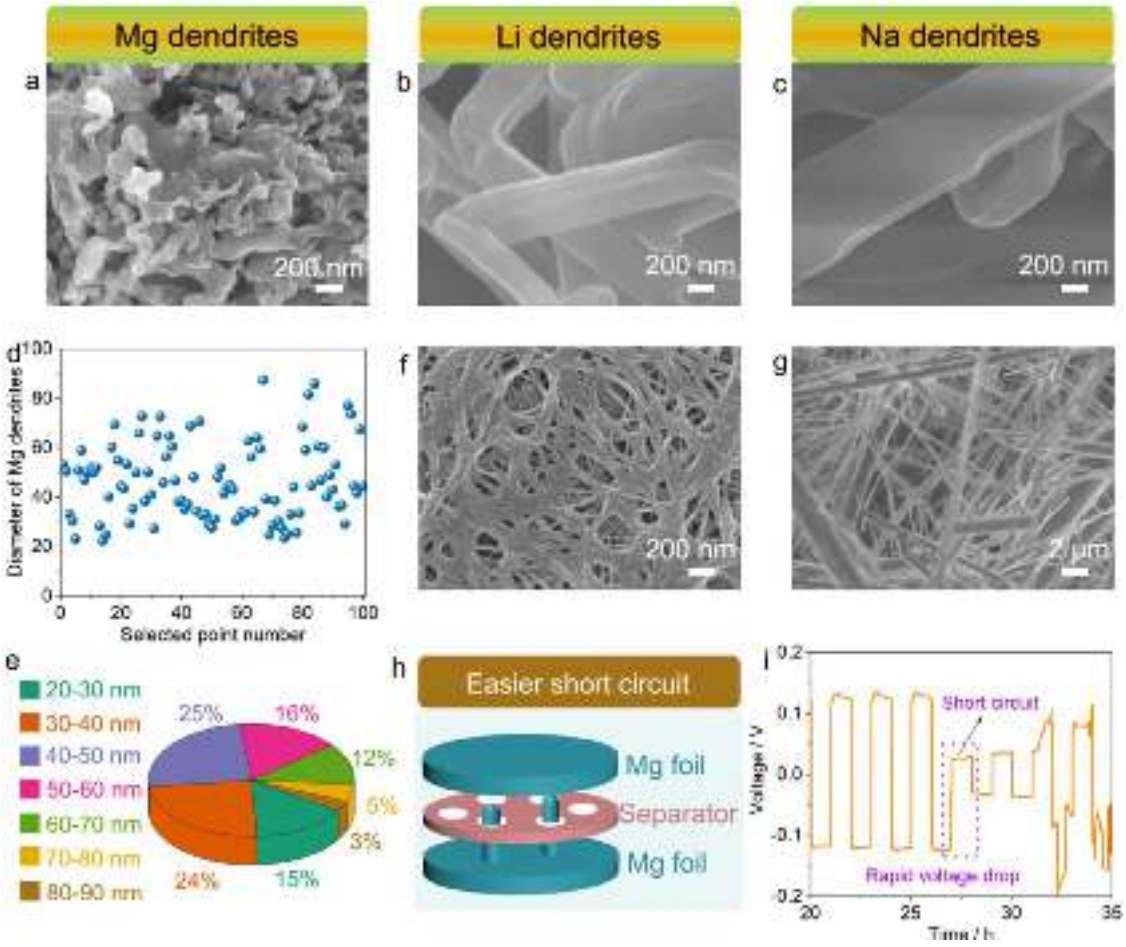

Fig. 7. (a–c) Top-view SEM images after depositing 2 mAh cm^{-2} of Mg, Li, and Na on Mg, Li, and Na electrodes at 0.5 mA cm^{-2}, respectively. (d) The diameter of Mg dendrites in the selected 100 points in Fig. S17. (e) The size distribution of Mg dendrites in the selected 100 points in Fig. S17. (f, g) Top-view SEM images of polyethylene and glass fiber separators, respectively. (h) A schematic showing nanoscale Mg dendrites could easily piece through the separators and cause short circuit. (i) Voltage-time curves of Mg symmetric cells selected in Fig. 6d showing the phenomenon of short circuit (1 mA cm^{-2}-1 mAh cm^{-2}) .

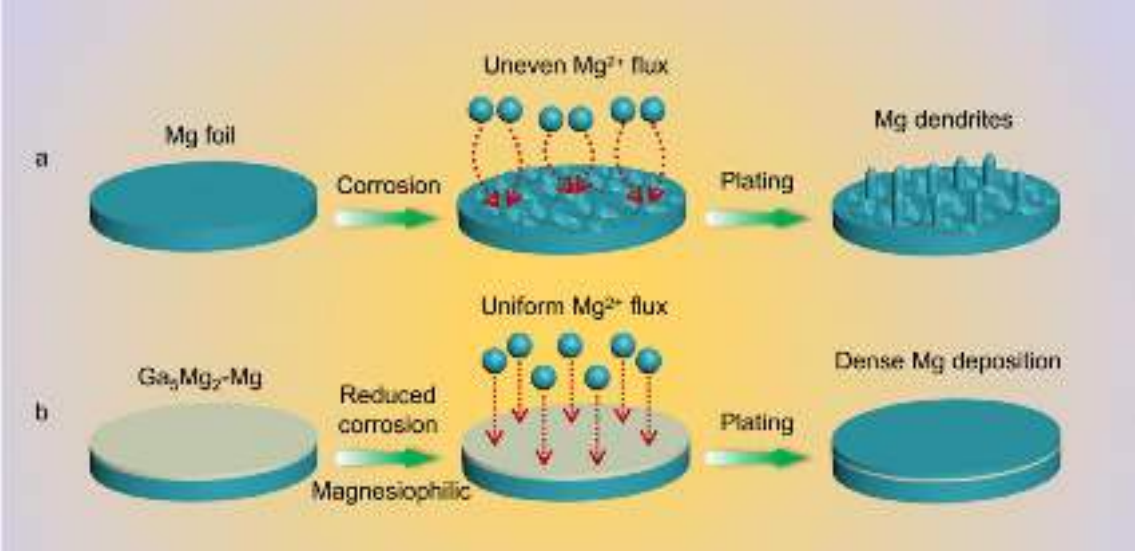

Fig. 8. (a, b) Schematics showing the electrochemical behaviors of Mg and Ga_5Mg_2-Mg electrodes, respectively.

than that on Ga_5Mg_2-Mg electrode, indicating the Ga_5Mg_2 alloy layer could effectively inhibit the electrolyte decomposition.

SEM was used to further investigate the features of Mg dendrites. It was found that the size of Mg dendrites was much smaller than that of Li and Na dendrites (Figs. 7a–c, S16). 100 points were selected to measure the diameter of Mg dendrites (Fig. S17). The diameter of most Mg dendrites was in 30–50 nm (Fig. 7d,e) and the average diameter was 46 nm. The size of Mg dendrites was much smaller than the pore diameter of separators (Fig. 7f,g). The so small-sized (nanoscale) Mg dendrites could easily pierce through the separators with large pore size and cause the internal short circuit of batteries (Fig. 7h,i). So Mg-metal batteries could easily become short-circuited, and this phenomenon has been found in previous reports [32]. Interestingly, the strategy proposed in this research could effectively inhibit the growth of Mg dendrites and avoid the easy short circuit of Mg-metal batteries.

After characterization and analysis, the mechanism of Ga_5Mg_2 layer could inhibit the growth of Mg dendrites was proposed (Fig. 8). Bare Mg electrode could be easily corroded by liquid electrolyte to form a defective surface, which could bring about inhomogeneous electric field distribution and then lead to uneven Mg^{2+} flux in the plating process. Uneven Mg^{2+} flux distribution on Mg electrode could lead to heterogeneous Mg nucleation and formation of Mg dendrites. While for Ga_5Mg_2-Mg, the corrosive-resistant and magnesiophilic Ga_5Mg_2 layer could not only relieve the interface corrosion from liquid electrolytes but also lower the Mg nucleation barrier to induce uniform Mg^{2+} flux and dense Mg deposition. As a result, the electrochemical performance of Ga_5Mg_2-Mg was much better than bare Mg electrode.

4. Conclusion

In summary, nanoscale Mg dendrites were detected in Mg metal anodes during the plating/stripping process and they could easily lead to the short circuit of Mg batteries. Accordingly, a simple liquid metal painting strategy was proposed to address the dendrite issue of Mg metal anodes. A Ga_5Mg_2 layer was spontaneously formed on the surface of Mg foil by the alloying reaction between metallic Ga and Mg. The Ga_5Mg_2 layer was stable, Mg^{2+}-conductive, corrosive-resistant, and magnesiophilic, finally leading to uniform and dendrite-free Mg deposition. The Ga_5Mg_2-Mg exhibited superior electrochemical performance both in symmetric cells and Mg-S full cells. Optimizing the thickness of Ga_5Mg_2 layer, modifying the composition of liquid electrolytes, or changing the kinds of liquid metals could possibly further improve the electrochemical performance of Mg-metal batteries, which should be further studied in the following research. We believe this research could enlighten related researchers and pave the way for high-energy Mg-metal batteries.

Declaration of Competing Interest

The authors declare no competing financial interest.

CRediT authorship contribution statement

Chuanliang Wei: Writing – original draft, Writing – review & editing. **Liwen Tan:** Data curation, Methodology, Writing – review & editing. **Yuchan Zhang:** Data curation, Methodology, Writing – review & editing. **Baojuan Xi:** Writing – review & editing. **Shenglin Xiong:** Writing – review & editing. **Jinkui Feng:** Visualization, Supervision, Writing – review & editing. **Yitai Qian:** Writing – review & editing.

Acknowledgments

This work was supported by the National Natural Science Foundation of China (No. 51972198; 62133007), Shenzhen Fundamental Research Program (No. JCYJ20190807093405503), Taishan Scholars Program of Shandong Province (No. tsqn201812002, ts20190908), the Natural Science Foundation of Shandong Province (No. ZR2020JQ19).

Supplementary materials

Supplementary material associated with this article can be found, in the online version, at doi:10.1016/j.ensm.2022.03.046.

References

[1] M. Armand, J.M. Tarascon, Building better batteries, Nature 451 (2008) 652–657, doi:10.1038/451652a.
[2] M. Li, J. Lu, Z. Chen, K. Amine, 30 years of lithium-ion batteries, Adv. Mater. 30 (2018) 1800561, doi:10.1002/adma.201800561.
[3] M. Winter, B. Barnett, K. Xu, Before Li ion batteries, Chem. Rev. 118 (2018) 11433–11456, doi:10.1021/acs.chemrev.8b00422.
[4] Y. Tian, G. Zeng, A. Rutt, T. Shi, H. Kim, J. Wang, J. Koettgen, Y. Sun, B. Ouyang, T. Chen, Z. Lun, Z. Rong, K. Persson, G. Ceder, Promises and challenges of next-generation "beyond Li-ion" batteries for electric vehicles and grid decarbonization, Chem. Rev. 121 (2021) 1623–1669, doi:10.1021/acs.chemrev.0c00767.
[5] C. Wei, Y. Tao, H. Fei, Y. An, Y. Tian, J. Feng, Y. Qian, Recent advances and perspectives in stable and dendrite-free potassium metal anodes, Energy Storage Mater. 30 (2020) 206–227, doi:10.1016/j.ensm.2020.05.018.

[6] C. Wei, L. Tan, Y. Zhang, K. Zhang, B. Xi, S. Xiong, J. Feng, Y. Qian, Covalent organic frameworks and their derivatives for better metal anodes in rechargeable batteries, ACS Nano 15 (2021) 12741–12767, doi:10.1021/acsnano.1c05497.

[7] C. Wei, H. Fei, Y. Tian, Y. An, H. Guo, J. Feng, Y. Qian, Isotropic Li nucleation and growth achieved by an amorphous liquid metal nucleation seed on MXene framework for dendrite-free Li metal anode, Energy Storage Mater. 26 (2020) 223–233, doi:10.1016/j.ensm.2020.01.005.

[8] C. Wei, Y. Wang, Y. Zhang, L. Tan, Y. Qian, Y. Tao, S. Xiong, J. Feng, Flexible and stable 3D lithium metal anodes based on self-standing MXene/COF frameworks for high-performance lithium-sulfur batteries, Nano Res. 14 (2021) 3576–3584, doi:10.1007/s12274-021-3433-9.

[9] C. Wei, Y. Zhang, Y. Tian, L. Tan, Y. An, Y. Qian, B. Xi, S. Xiong, J. Feng, Y. Qian, Design of safe, long-cycling and high-energy lithium metal anodes in all working conditions: progress, challenges and perspectives, Energy Storage Mater. 38 (2021) 157–189, doi:10.1016/j.ensm.2021.03.006.

[10] C. Wei, L. Tan, Y. Zhang, B. Xi, S. Xiong, J. Feng, MXene/organics heterostructures enable ultrastable and high-rate lithium/sodium batteries, ACS Appl. Mater. Interfaces 14 (2022) 2979–2988, doi:10.1021/acsami.1c22787.

[11] C. Wei, L. Tan, Y. Zhang, S. Xiong, J. Feng, Metal-organic frameworks and their derivatives in stable Zn metal anodes for aqueous Zn-ion batteries, ChemPhysMater (2022), doi:10.1016/j.chphma.2021.09.003.

[12] C. You, X. Wu, X. Yuan, Y. Chen, L. Liu, Y. Zhu, L. Fu, Y. Wu, Y. Guo, T.V. Ree, Advances in rechargeable Mg batteries, J. Mater. Chem. A 8 (2020) 25601–25625, doi:10.1039/d0ta09330k.

[13] J. Zhang, Z. Chang, Z. Zhang, A. Du, S. Dong, Z. Li, G. Li, G. Cui, Current design strategies for rechargeable magnesium-based batteries, ACS Nano 15 (2021) 15594–15624, doi:10.1021/acsnano.1c06530.

[14] P. Saha, M.K. Datta, O.I. Velikokhatnyi, A. Manivannan, D. Alman, P.N. Kumta, Rechargeable magnesium battery: current status and key challenges for the future, Prog. Mater. Sci. 66 (2014) 1–86, doi:10.1016/j.pmatsci.2014.04.001.

[15] C. Pei, F. Xiong, Y. Yin, Z. Liu, H. Tang, R. Sun, Q. An, L. Mai, Recent progress and challenges in the optimization of electrode materials for rechargeable magnesium batteries, Small 17 (2021) 2004108, doi:10.1002/smll.202004108.

[16] Q. Guo, W. Zeng, S. Liu, Y. Li, J. Xu, J. Wang, Y. Wang, Recent developments on anode materials for magnesium-ion batteries: a review, Rare Met. 40 (2021) 290–308, doi:10.1007/s12598-020-01493-3.

[17] D. Li, Y. Yuan, J. Liu, M. Fichtner, F. Pan, A review on current anode materials for rechargeable Mg batteries, J. Magnes. Alloy. 8 (2020) 963–979, doi:10.1016/j.jma.2020.09.017.

[18] F. Liu, T. Wang, X. Liu, L. Fan, Challenges and recent progress on key materials for rechargeable magnesium batteries, Adv. Energy Mater. 11 (2021) 2000787, doi:10.1002/aenm.202000787.

[19] C. Wei, Y. Tao, Y. An, Y. Tian, Y. Zhang, J. Feng, Y. Qian, Recent advances of emerging 2D MXene for stable and dendrite-free metal anodes, Adv. Funct. Mater. 30 (2020) 2004613, doi:10.1002/adfm.202004613.

[20] Y. Zhang, H. Geng, W. Wei, J. Ma, L. Chen, C.C. Li, Challenges and recent progress in the design of advanced electrode materials for rechargeable Mg batteries, Energy Storage Mater. 20 (2019) 118–138, doi:10.1016/j.ensm.2018.11.033.

[21] L. Kong, C. Yan, J. Huang, M. Zhao, M. Titirici, R. Xiang, Q. Zhang, A review of advanced energy materials for magnesium-sulfur batteries, Energy Environ. Mater. 1 (2018) 100–112, doi:10.1002/eem2.12012.

[22] L. Li, H. Chen, E. He, L. Wang, T. Ye, J. Lu, Y. Jiao, J. Wang, R. Gao, H. Peng, Y. Zhang, High-energy-density magnesium-air battery based on dual-layer gel electrolyte, Angew. Chem. Int. Ed. 60 (2021) 15317–15322, doi:10.1002/anie.202104536.

[23] J. Kim, A. Seong, Y. Yang, S. Joo, C. Kim, D.H. Jeon, L. Dai, G. Kim, Indirect surpassing CO_2 utilization in membrane-free CO_2 battery, Nano Energy 82 (2021) 105741, doi:10.1016/j.nanoen.2020.105741.

[24] R. Attias, M. Salama, B. Hirsch, Y. Goffer, D. Aurbach, Anode-electrolyte interfaces in secondary magnesium batteries, Joule 3 (2019) 27–52, doi:10.1016/j.joule.2018.10.028.

[25] J. Shi, J. Zhang, J. Guo, J. Lu, Interfaces in rechargeable magnesium batteries, Nanoscale Horiz. 5 (2020) 1467–1475, doi:10.1039/d0nh00379d.

[26] Z. Liang, C. Ban, Strategies to enable reversible magnesium electrochemistry: from electrolytes to artificial solid-electrolyte interphases, Angew. Chem. Int. Ed. 60 (2021) 11036–11047, doi:10.1002/anie.202006472.

[27] M. Jackle, K. Helmbrecht, M. Smits, D. Stottmeister, A. Groß, Self-diffusion barriers: possible descriptors for dendrite growth in batteries? Energy Environ. Sci. 11 (2018) 3400–3407, doi:10.1039/c8ee01448e.

[28] C. Ling, D. Banerjee, M. Matsui, Study of the electrochemical deposition of Mg in the atomic level: why it prefers the non-dendritic morphology, Electrochim. Acta 76 (2012) 270–274, doi:10.1016/j.electacta.2012.05.001.

[29] M. Matsui, Study on electrochemically deposited Mg metal, J. Power Sources 196 (2011) 7048–7055, doi:10.1016/j.jpowsour.2010.11.141.

[30] A. Hagopian, D. Kopac, J. Filhol, A.K. Lautar, Morphology evolution and dendrite growth in Li- and Mg-metal batteries: a potential dependent thermodynamic and kinetic multiscale ab initio study, Electrochim. Acta 353 (2020) 136493, doi:10.1016/j.electacta.2020.136493.

[31] R. Davidson, A. Verma, D. Santos, F. Hao, C.D. Fincher, D. Zhao, V. Attari, P. Schofield, J.V. Buskirk, A. Fraticelli-Cartagena, T.E.G. Alivio, R. Arroyave, K. Xie, M. Pharr, P.P. Mukherjee, S. Banerjee, Mapping mechanisms and growth regimes of magnesium electrodeposition at high current densities, Mater. Horiz. 7 (2020) 843–854, doi:10.1039/c9mh01367a.

[32] J. Eaves-Rathert, K. Moyer, M. Zohair, C.L. Pint, Kinetic-versus diffusion-driven three-dimensional growth in magnesium metal battery anodes, Joule 4 (2020) 1324–1336, doi:10.1016/j.joule.2020.05.007.

[33] R. Davidson, A. Verma, D. Santos, F. Hao, C. Fincher, S. Xiang, J.V. Buskirk, K. Xie, M. Pharr, P.P. Mukherjee, S. Banerjee, Formation of magnesium dendrites during electrodeposition, ACS Energy Lett. 4 (2019) 375–376, doi:10.1021/acsenergylett.8b02470.

[34] F. Hao, A. Verma, PP. Mukherjee, Electrodeposition stability of metal electrodes, Energy Storage Mater. 20 (2019) 1–6, doi:10.1016/j.ensm.2019.05.004.

[35] MS. Ding, T. Diemant, R.J Behm, S. Passerini, GA. Giffin, Dendrite growth in Mg metal cells containing $Mg(TFSI)_2$/glyme electrolytes, J. Electrochem. Soc. 165 (2018) A1983–A1990, doi:10.1149/2.1471809jes.

[36] D. Aurbach, Z. Lu, A. Schechter, Y. Gofer, H. Gizbar, R. Turgeman, Y. Cohen, M. Moshkovich, E. Levi, Prototype systems for rechargeable magnesium batteries, Nature 407 (2000) 724–727, doi:10.1038/35037553.

[37] S. Hou, X. Ji, K. Gaskell, P. Wang, L. Wang, J. Xu, R. Sun, O. Borodin, C. Wang, Solvation sheath reorganization enables divalent metal batteries with fast interfacial charge transfer kinetics, Science 374 (2021) 172–178, doi:10.1126/science.abg3954.

[38] R. Deivanayagam, B.J. Ingram, R. Shahbazian-Yassar, Progress in development of electrolytes for magnesium batteries, Energy Storage Mater. 21 (2019) 136–153, doi:10.1016/j.ensm.2019.05.028.

[39] H. Wang, X. Feng, Y. Chen, Y. Liu, K.S. Han, M. Zhou, M.H. Engelhard, V. Murugesan, R.S. Assary, T.L. Liu, W. Henderson, Z. Nie, M. Gu, J. Xiao, C. Wang, K. Persson, D. Mei, J. Zhang, K.T. Mueller, J. Guo, K. Zavadil, Y. Shao, J. Liu, Reversible electrochemical interface of Mg metal and conventional electrolyte enabled by intermediate adsorption, ACS Energy Lett. 5 (2020) 200–206, doi:10.1021/acsenergylett.9b02211.

[40] D. Nguyen, A.Y.S. Eng, R. Horia, Z. Sofer, A.D. Handoko, M. Ng, Z.W. Seh, Rechargeable magnesium batteries enabled by conventional electrolytes with multifunctional organic chloride additives, Energy Storage Mater. 45 (2022) 1120–1132, doi:10.1016/j.ensm.2021.11.011.

[41] R. Horia, D. Nguyen, A.Y.S. Eng, Z.W. Seh, Using a chloride-free magnesium battery electrolyte to form a robust anode-electrolyte nanointerface, Nano Lett. 21 (2021) 8220–8228, doi:10.1021/acs.nanolett.1c02655.

[42] D. Nguyen, A.Y.S. Eng, M. Ng, V. Kumar, Z. Sofer, A.D. Handoko, G.S. Subramanian, Z.W. Seh, A high-performance magnesium triflate-based electrolyte for rechargeable magnesium batteries, Cell Rep. Phys. Sci. 1 (2020) 100265, doi:10.1016/j.xcrp.2020.100265.

[43] K. Tang, A. Du, S. Dong, Z. Cui, X. Liu, C. Lu, J. Zhao, X. Zhou, G. Cui, A stable solid electrolyte interphase for magnesium metal anode evolved from a bulky anion lithium salt, Adv. Mater. 32 (2020) 1904987, doi:10.1002/adma.201904987.

[44] S. Son, T. Gao, S.P. Harvey, K.X. Steirer, A. Stokes, A. Norman, C. Wang, A. Cresce, K. Xu, C. Ban, An artificial interphase enables reversible magnesium chemistry in carbonate electrolytes, Nat. Chem. 10 (2018) 532–539, doi:10.1038/s41557-018-0019-6.

[45] R. Lv, X. Guan, J. Zhang, Y. Xia, J. Luo, Enabling Mg metal anodes rechargeable in conventional electrolytes by fast ionic transport interphase, Natl. Sci. Rev. 7 (2020) 333–341, doi:10.1093/nsr/nwz157.

[46] B. Li, R. Masse, C. Liu, Y. Hu, W. Li, G. Zhang, G. Cao, Kinetic surface control for improved magnesium-electrolyte interfaces for magnesium ion batteries, Energy Storage Mater. 22 (2019) 96–104, doi:10.1016/j.ensm.2019.06.035.

[47] J. Zhang, X. Guan, R. Lv, D. Wang, P. Liu, J. Luo, Rechargeable Mg metal batteries enabled by a protection layer formed *in vivo*, Energy Storage Mater. 26 (2020) 408–413, doi:10.1016/j.ensm.2019.11.012.

[48] X. Li, T. Gao, F. Han, Z. Ma, X. Fan, S. Hou, N. Eidson, W. Li, C. Wang, Reducing Mg anode overpotential via ion conductive surface layer formation by iodine additive, Adv. Energy Mater. 8 (2018) 1701728, doi:10.1002/aenm.201701728.

[49] Y. Zhao, A. Du, S. Dong, F. Jiang, Z. Guo, X. Ge, X. Qu, X. Zhou, G. Cui, A bismuth-based protective layer for magnesium metal anode in noncorrosive electrolytes, ACS Energy Lett. 6 (2021) 2594–2601, doi:10.1021/acsenergylett.1c01243.

[50] H. Park, H.K. Lim, S.H. Oh, J. Park, H.D. Lim, K. Kang, Tailoring ion-conducting interphases on magnesium metals for high-efficiency rechargeable magnesium metal batteries, ACS Energy Lett. 5 (2020) 3733–3740, doi:10.1021/acsenergylett.0c02102.

[51] Y. Li, X. Zhou, J. Hu, Y. Zheng, M. Huang, K. Guo, C. Li, Reversible Mg metal anode in conventional electrolyte enabled by durable heterogeneous SEI with low surface diffusion barrier, Energy Storage Mater. 46 (2022) 1–9, doi:10.1016/j.ensm.2021.12.023.

[52] E. Sahadeo, G. Rubloff, S.B. Lee, C. Lin, Al_2O_3 thin films on magnesium: assessing the impact of an artificial solid electrolyte interphase, Front. Energy Res. 9 (2021) 618368, doi:10.3389/fenrg.2021.618368.

[53] Y. Zhang, J. Li, W. Zhao, H. Dou, X. Zhao, Y. Liu, B. Zhang, X. Yang, Defect-free metal-organic framework membrane for precise ion/solvent separation toward highly stable magnesium metal anode, Adv. Mater. 34 (2022) 2108114, doi:10.1002/adma.202108114.

[54] J. Wang, W. Zhao, H. Dou, B. Wan, Y. Zhang, W. Li, X. Zhao, X. Yang, Electrostatic shielding guides lateral deposition for stable interphase toward reversible magnesium metal anodes, ACS Appl. Mater. Interfaces 12 (2020) 19601–19606, doi:10.1021/acsami.0c03603.

[55] H. Dou, X. Zhao, Y. Zhang, W. Zhao, Y. Yan, Z. Ma X. Wang, X. Yang, Revisiting the degradation of solid/electrolyte interfaces of magnesium metal anodes: decisive role of interfacial composition, Nano Energy 86 (2021) 106087, doi:10.1016/j.nanoen.2021.106087.

[56] Z. Song, Z. Zhang, A. Du, S. Dong, G. Li, G. Cui, Uniform magnesium electrodeposition via synergistic coupling of current homogenization, geometric confinement, and chemisorption effect, Adv. Mater. 33 (2021) 2100224, doi:10.1002/adma.202100224.

[57] H. Lim, D.H. Kim, S. Park, M.E. Lee, H. Jin, S. Yu, S.H. Oh, Y.S. Yun, Magnesiophilic graphitic carbon nanosubstrate for highly efficient and fast-rechargeable Mg metal batteries, ACS Appl. Mater. Interfaces 11 (2019) 38754–38761, doi:10.1021/acsami.9b13447.

[58] B. Wan, H. Dou, X. Zhao, J. Wang, W. Zhao, M. Guo, Y. Zhang, J. Li, Z. Ma, X. Yang, Three-dimensional magnesiophilic scaffolds for reduced passivation toward high-rate Mg metal anodes in a noncorrosive electrolyte, ACS Appl. Mater. Interfaces 12 (2020) 28298–28305, doi:10.1021/acsami.0c07213.

[59] O. Tutusaus, R. Mohtadi, N. Singh, T.S. Arthur, F. Mizuno, Study of electrochemical phenomena observed at the Mg metal/electrolyte interface, ACS Energy Lett. 2 (2017) 224–229, doi:10.1021/acsenergylett.6b00549.

[60] J.H. Kwak, Y. Jeoun, S.H. Oh, S. Yu, J. Lim, Y. Sung, S. Yu, H. Lim, Operando visualization of morphological evolution in Mg metal anode: insight into dendrite suppression for stable Mg metal batteries, ACS Energy Lett. 7 (2022) 162–170, doi:10.1021/acsenergylett.1c02486.

[61] X. Chen, S. Wei, F. Tong, M.P. Taylor, P. Cao, Electrochemical performance of Mg-Sn alloy anodes for magnesium rechargeable battery, Electrochim. Acta 398 (2021) 139336, doi:10.1016/j.electacta.2021.139336.

[62] L. Wang, S.S. Welborn, H. Kumar, M. Li, Z. Wang, V.B. Shenoy, E. Detsi, High-rate and long cycle-life alloy-type magnesium-ion battery anode enabled through (De)magnesiation-induced near-room-temperature solid-liquid phase transformation, Adv. Energy Mater. 9 (2019) 1902086, doi:10.1002/aenm.201902086.

[63] P.W. Jaschin, Y. Gao, Y. Li, S. Bo, A materials perspective on magnesium-ion-based solid-state electrolytes, J. Mater. Chem. A 8 (2020) 2875–2897, doi:10.1039/c9ta11729f.

[64] C. Wei, H. Fei, Y. Tian, Y. An, G. Zeng, J. Feng, Y. Qian, Room-temperature liquid metal confned in MXene paper as a flexible, freestanding, and binder-free anode for next-generation lithium-ion batteries, Small 15 (2019) 1903214, doi:10.1002/smll.201903214.

[65] C. Wei, L. Tan, Y. Tao, Y. An, Y. Tian, H. Jiang, J. Feng, Y. Qian, Interfacial passivation by room-temperature liquid metal enabling stable 5 V-class lithium-metal batteries in commercial carbonate-based electrolyte, Energy Storage Mater. 34 (2021) 12–21, doi:10.1016/j.ensm.2020.09.006.

[66] C. Wei, H. Fei, Y. An, Y. Tao, J. Feng, Y. Qian, Uniform Li deposition by regulating the initial nucleation barrier via a simple liquid-metal coating for a dendrite-free Li-metal anode, J. Mater. Chem. A 7 (2019) 18861–18870, doi:10.1039/C9TA06663B.

[67] C. Song, Y. Yuan, D. Gu, T. Chen, Y. Liu, A. Tang, L. Wu, D. Li, F. Pan, The evaluation of Mg-Ga compounds as electrode materials for Mg-ion batteries via ab initio simulation, J. Electrochem. Soc. 168 (2021) 110539, doi:10.1149/1945-7111/ac3936.

[68] M.J. Regan, H. Tostmann, P.S. Pershan, X-ray study of the oxidation of liquid-gallium surfaces, Phys. Rev. B 55 (1997) 10786–10790, doi:10.1103/PhysRevB.55.10786.

[69] H. Zhong, Y. Wu, F. Ding, L. Sang, Y. Mai, An artificial Li-Al interphase layer on Li-B alloy for stable lithium metal anode, Electrochim. Acta 304 (2019) 255–262, doi:10.1016/j.electacta.2019.03.009.

[70] B. Han, D. Xu, S. Chi, D. He, Z. Zhang, L. Du, M. Gu, C. Wang, H. Meng, K. Xu, Z. Zheng, Y. Deng, 500 Wh kg^{-1} class Li metal battery enabled by a self-organized core-shell composite anode, Adv. Mater. 32 (2020) 2004793, doi:10.1002/adma.202004793.

[71] J. Niu, Z. Zhang, D. Aurbach, Alloy anode materials for rechargeable Mg ion batteries, Adv. Energy Mater. 10 (2020) 2000697, doi:10.1002/aenm.202000697.

[72] C. Wei, L. Tan, Y. Zhang, H. Jiang, B. Xi, S. Xiong, J. Feng, Room-temperature liquid metal engineered iron current collector enables stable and dendrite-free sodium metal batteries in carbonate electrolytes, J. Mater. Sci. Technol. 115 (2022) 156–165, doi:10.1016/j.jmst.2021.11.034.

[73] D. Nguyen, R. Horia, A.Y.S. Eng, S. Song, Z.W. Seh, Material design strategies to improve the performance of rechargeable magnesium-sulfur batteries, Mater. Horiz. 8 (2021) 830–853, doi:10.1039/D0MH01403F.

[74] M.D. Regulacio, D. Nguyen, R. Horia, Z.W. Seh, Designing nanostructured metal chalcogenides as cathode materials for rechargeable magnesium batteries, Small 17 (2021) 2007683, doi:10.1002/smll.202007683.

[75] Y. Li, P. Zuo, R. Li, M. He, Y. Ma, Y. Shi, X. Cheng, C. Du, G. Yin, Electrochemically-driven interphase conditioning of magnesium electrode for magnesium sulfur batteries, J. Energy Chem. 37 (2019) 215–219, doi:10.1016/j.jechem.2019.03.032.

[76] W. Wang, H. Yuan, Y. NuLi, J. Zhou, J. Yang, J. Wang, Sulfur@microporous carbon cathode with a high sulfur content for magnesium-sulfur batteries with nucleophilic electrolytes, J. Phys. Chem. C 122 (2018) 26764–26776, doi:10.1021/acs.jpcc.8b09003.

[77] H. Fan, Z. Zheng, L. Zhao, W. Li, J. Wang, M. Dai, Y. Zhao, J. Xiao, G. Wang, X. Ding, H. Xiao, J. Li, Y. Wu, Y. Zhang, Extending cycle life of Mg/S battery by activation of Mg anode/electrolyte interface through an LiCl-assisted $MgCl_2$ solubilization mechanism, Adv. Funct. Mater. 30 (2020) 1909370, doi:10.1002/adfm.201909370.

[78] P. Wang, M.R. Buchmeiser, Rechargeable magnesium-sulfur battery technology: state of the art and key challenges, Adv. Funct. Mater. 29 (2019) 1905248, doi:10.1002/adfm.201905248.

[79] M. Rashad, M. Asif, Z. Ali, Quest for magnesium-sulfur batteries: current challenges in electrolytes and cathode materials developments, Coordin. Chem. Rev. 415 (2020) 213312, doi:10.1016/j.ccr.2020.213312.

[80] Q. Zou, Y. Sun, Z. Liang, W. Wang, Y. Lu, Achieving efficient magnesium-sulfur battery chemistry via polysulfide mediation, Adv. Energy Mater. 11 (2021) 2101552, doi:10.1002/aenm.202101552.